HHS Public Access

Author manuscript

Cell Rep. Author manuscript; available in PMC 2016 December 06.

Published in final edited form as:

Cell Rep. 2016 November 15; 17(8): 1923–1933. doi:10.1016/j.celrep.2016.10.072.

Alternative Splicing of Four Trafficking Genes Regulates Myofiber Structure and Skeletal Muscle Physiology

Jimena Giudice[1,2,3,4,*], **James A. Loehr**[5], **George G. Rodney**[5], and **Thomas A. Cooper**[1,5,6,7,*]

[1]Department of Pathology & Immunology, Baylor College of Medicine, Houston, TX 77030, USA

[2]Department of Cell Biology and Physiology, School of Medicine, The University of North Carolina at Chapel Hill, Chapel Hill, NC 27599, USA

[3]McAllister Heart Institute, The University of North Carolina at Chapel Hill, Chapel Hill, NC 27599, USA

[4]Curriculum in Genetics and Molecular Biology, The University of North Carolina at Chapel Hill, Chapel Hill, NC 27599, USA

[5]Department of Molecular Physiology & Biophysics, Baylor College of Medicine, Houston, TX 77030, USA

[6]Department of Molecular & Cellular Biology, Baylor College of Medicine, Houston, TX 77030, USA

SUMMARY

During development, transcriptional and post-transcriptional networks are coordinately regulated to drive organ maturation. Alternative splicing contributes by producing temporal-specific protein isoforms. We previously found that genes undergoing splicing transitions during mouse postnatal heart development are enriched for vesicular trafficking and membrane dynamics functions. Here, we show that adult trafficking isoforms are also expressed in adult skeletal muscle and hypothesize that striated muscle utilizes alternative splicing to generate specific isoforms required for function of adult tissue. We deliver morpholinos into *flexor digitorum brevis* muscles in adult mice to redirect splicing of four trafficking genes to the fetal isoforms. The splicing switch results in multiple structural and functional defects, including transverse tubule (T-tubule) disruption and dihydropyridine receptor alpha (DHPR) and Ryr1 mislocalization, impairing excitation-contraction coupling, calcium handling, and force generation. The results demonstrate a previously unrecognized role for trafficking functions in adult muscle tissue homeostasis and a specific requirement for the adult splice variants.

[*]Correspondence: jimena_giudice@med.unc.edu (J.G.), tcooper@bcm.edu (T.A.C.).
[7]Lead Contact

SUPPLEMENTAL INFORMATION

Supplemental Information includes Supplemental Experimental Procedures, five figures, and two tables and can be found with this article online at http://dx.doi.org/10.1016/j.celrep.2016.10.072.

AUTHOR CONTRIBUTIONS

J.G. and T.A.C. developed the project. J.G., J.A.L., G.G.R., and T.A.C. designed the experiments. J.A.L. performed force and calcium measurements. J.G. performed the rest of the experiments. J.G., J.A.L., G.G.R., and T.A.C. analyzed and discussed the data. J.G. wrote the manuscript draft. J.A.L., G.G.R., and T.A.C. edited and contributed to the final manuscript. All authors revised and approved the submitted manuscript.

In Brief

Trafficking genes are regulated by alternative splicing during postnatal heart development. Here, Giudice et al. redirect splicing of four trafficking genes to their fetal isoforms in mice and show that the adult isoforms are required for calcium handling and excitation contraction coupling in adult striated muscle.

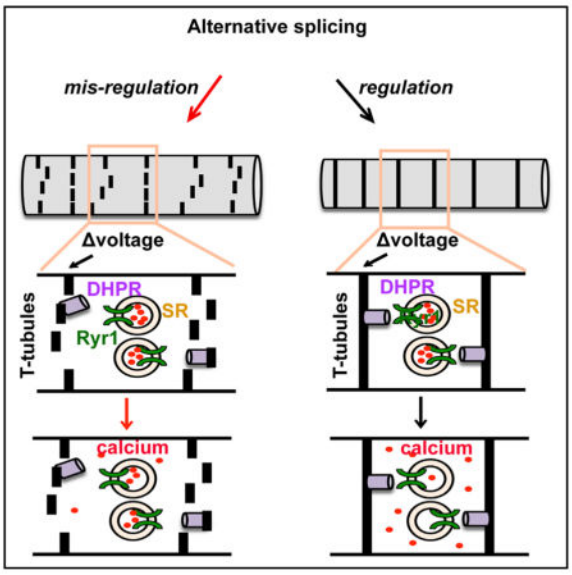

INTRODUCTION

When genomes of different species were sequenced, the most important observation was that organism complexity does not correlate with the number of genes encoding for proteins (Blencowe, 2006). This finding suggests that regulatory mechanisms have played a role in gene function diversification during evolution (Blencowe, 2006). Alternative splicing (AS) is a post-transcriptional mechanism by which individual genes produce more than one mRNA transcript, allowing the expression of multiple protein isoforms with diverse features from single genes. Approximately 90%–95% of human genes undergo AS (Pan et al., 2008; Wang et al., 2008), consistent with the increased cellular and functional complexity in higher eukaryotes. Brain, heart, and skeletal muscle have the most tissue-specific AS and show the most conserved AS signatures in mammals and chickens (Merkin et al., 2012).

We previously identified extensive cell-type-specific AS transitions during postnatal development in freshly isolated mouse cardiomyocytes and cardiac fibroblasts (Giudice et al., 2014). Whereas AS transitions continued throughout the postnatal period in cardiac fibroblasts, in cardiomyocytes, most transitions were complete within the first 4 weeks after birth (Giudice et al., 2014). We have shown that, specifically during cardiomyocyte development, AS regulates trafficking and membrane dynamics genes (Giudice et al., 2014), leading us to ask about the functional role of this regulatory network.

Trafficking and membrane dynamics are likely to play important roles in striated muscle biology. The first 3 to 4 postnatal weeks are when striated muscle cells mature the internal

cellular architecture required for adult contractile functions. Adult striated muscle cells are large and thus require specialized membrane compartments for simultaneous contraction throughout the cell. Transverse tubules (T-tubules) are formed by invaginations of the plasma membrane to allow access of the environmental signals and propagation of depolarization deep into the cells. T-tubules are critical structures for excitation-contraction coupling (ECC), in which external signals trigger membrane depolarization and increased cytoplasmic calcium concentration leads to actin and myosin filament translocations and contraction. Contractile muscle functions require a range of trafficking and membrane dynamics processes, such as formation and maintenance of the membrane invaginations constituting the T-tubules, proper localization of receptors and ion channels within the T-tubules and the sarcoplasmic reticulum(SR), as well as timely internalization, recycling, and degradation of these proteins.

The importance of the above-mentioned processes in striated muscle is highlighted by the numerous human mutations in trafficking and membrane dynamics genes causing muscle and cardiac diseases (Dowling et al., 2008; Sigismund et al., 2012). Mutations in caveolin 3 gene (*CAV3*) are linked to muscular dystrophy limb-girdle type 1C and other muscle disorders. Mutations in the bridging integrator 1 (*BIN1*) and dynamin 2 (*DNM2*) genes cause centronuclear myopathy, whereas dysferlin (*DYSF*) and myotubularin (*MTM1*) mutations cause dysferlinopathies and myotubular myopathies, respectively. Human mutations in ryanodine receptor type 1 (*RYR1*) and 2 (*RYR2*) genes are linked to sporadic centronuclear myopathy and cardiac pathologies, respectively (Dowling et al., 2008; Sigismund et al., 2012).

We hypothesize that AS regulation of trafficking genes contributes to adult muscle function and homeostasis. Previously, we showed that, in heart, reinduction of the RNA-binding protein CELF1 in adult mice using an inducible transgenic model for cardiomyocyte-specific expression reverts the AS of trafficking genes to fetal patterns and these animals exhibit serious disruptions in T-tubule organization and calcium handling (Giudice et al., 2014). However, in that study, we were not able to directly link the AS-trafficking network to the physiological effects because CELF1 re-expression induces transcriptional and post-transcriptional changes separate from the AS misregulation of trafficking events. Here, we (1) revert endogenous AS toward fetal patterns in adults, (2) modulate AS in vivo to determine the physiological consequences on striated muscles, (3) target specific AS events directly rather than approaches that affect a large number of genes and post-transcriptional processes, and (4) modulate AS of multiple events simultaneously to determine the impact of coordinated AS of functionally related proteins.

We found that four AS events regulated during cardiomyocyte postnatal development (Giudice et al., 2014) expressed the long isoform in adult skeletal muscle, in particular in the *flexor digitorum brevis* (FDB) muscle located in mouse footpad. The genes exhibiting similar AS patterns in FDB and heart are the synaptosomal-associated protein 23 (Snap23) (exon of 33 nt), the Cdc42-interacting protein 4 (Trip10/Cip4) (exon of 168 nt), the clathrin heavy chain (Cltc) (exon of 21 nt), and the transmembrane emp24 domain-containing protein 2 (Tmed2) (exon of 21 nt) (Giudice et al., 2014). Tmed2 regulates protein-cargo selection and vesicle budding; however, the striated muscle functions are unknown.

Homozygous Tmed2 mouse knockout embryos die at midgestation, exhibiting developmental delay by embryonic day 8.5, abnormal heart looping, and absence of the placenta labyrinth layer (Jerome-Majewska et al., 2010). Cltc is the main player in clathrin-mediated endocytosis and is required for costamere organization through actin scaffolding (Vassilopoulos et al., 2014). Snap23, a SNARE complex member, is involved in glucose metabolism and Glut4 dynamics in adipocytes (Foster et al., 1999; Kawanishi et al., 2000) and insulin resistance in diabetic skeletal muscle (Boström et al., 2010) and cardiomyocytes (Boström et al., 2007). Trip10/Cip4 is a member of the F-Bar domain family proteins, specifically the Toca subfamily (Toca1, Fbp17/Fnbp1, and Cip4). Trip10/Cip4 regulates membrane deformation and tubulation and vesicular trafficking. Trip10/Cip4 is associated with developmental disorders inhibiting actin nucleation of embryonic morphogenesis in *Drosophila* (Yan et al., 2013) and is required for hypertrophic growth of rat neonatal cardiomyocytes (Rusconi et al., 2013).

The functional differences of the short (only isoforms expressed in neonates) and the long (gradually expressed during development) isoforms for these genes are unknown as well as the overall function of the majority of these trafficking-related proteins in the context of striated muscle biology. To investigate the role of the AS isoforms of Trip10, Snap23, Cltc, and Tmed2 in skeletal muscle physiology, we used morpholino (MO) antisense oligonucleotides to simultaneously redirect AS of all four exons in FDB muscles of adult mice. Three to four weeks after MO delivery, we observed the predominant expression of the short isoforms of Trip10, Snap23, Cltc, and Tmed2. Importantly, the isoform transition for endogenous gene products was accomplished without a change in overall mRNA levels, avoiding the effects of knockdown or overexpression. Muscles from these animals exhibited enlarged myofibers but reduced force generation and calcium release. T-tubules were disorganized, and localization of the Ryr1 was disrupted, altering its colocalization with the voltage sensor dihydropyridine receptor alpha (DHPR). Ultra-structural analysis by electron microscopy revealed the presence of vesicle-like structures and some abnormalities in mitochondria localization along the Z lines of muscle fibers. The results demonstrate a previously unknown role for protein isoform transitions of trafficking genes in maintaining T-tubule structure and contractile functions in adult skeletal muscles.

RESULTS

Snap23, Trip10, Cltc, and Tmed2 Undergo AS in Adult FDBs

During heart development, trafficking and membrane dynamics genes are the most significantly enriched among those regulated by AS within the first weeks after birth (Giudice et al., 2014). AS transitions in trafficking genes involve small exons encoding in frame peptides with unknown effects on protein function and structure. This is consistent with other studies showing that tissue-specific AS is enriched for segments encoding small disordered peptides that impact protein-protein interaction networks (Buljan et al., 2012; Ellis et al., 2012). Alternative exons tend to be skipped in neonatal cardiomyocytes but show inclusion in adults (Giudice et al., 2014). This developmental regulation was cell type specific in heart: present in cardiomyocytes and absent in cardiac fibroblasts (Giudice et al., 2014). We evaluated by RT-PCR assays the splicing of alternative exons from ten trafficking

genes that were regulated during postnatal heart and skeletal muscle development to identify those also included in adult FDB muscles. We observed that the long-mRNA transcripts of four trafficking genes (Snap23, Trip10, Cltc, and Tmed2) were also expressed in adult FDB skeletal muscles (Figure 1A). These events were selected to determine the consequences of AS redirection because our goal is to induce exon skipping in adult FBDs. Therefore, we need to have high levels of inclusion as our basal condition to ask what the physiological role is in the inclusion of those exons in adults compared to their exclusion in neonates.

The percentage of inclusion of the alternative exons in FDB muscles was either higher (Trip10 and Snap23) or lower (Cltc and Tmed2) than in adult heart; but for all four trafficking events, we observed the presence of the long isoforms in the FDBs. FDB muscles are extremely small, making it difficult to evaluate AS patterns at neonatal stages as we previously did for heart. Therefore, although not ideal, we evaluated developmental AS patterns of these events in other skeletal muscle tissues, observing transitions similar to those observed in heart development (Figure 1B). Taken together, these observations led us to hypothesize that short- and long-AS isoforms of these proteins play a functional role in adult striated muscle. To test this hypothesis, we modulated the four AS events simultaneously in vivo and evaluated muscle structure and function in FDBs because (1) we observed high levels of inclusion of the alternative exons in adults and (2) AS modulation is feasible and reproducible in these small and accessible muscles.

MO Delivery In Vivo Led to a Preferential Expression of Short AS Isoforms

We designed MO targeting the 3′ and/or 5′ splice sites of the alternative exons of Snap23 (33 nt), Trip10 (168 nt), Cltc (21 nt), and Tmed2 (21 nt). We injected and electroporated the mix of five MOs targeting the four events simultaneously, and as control, we delivered an equivalent amount of a control MO. All analyses presented were performed 23–28 days after MO delivery to allow time for FDB muscle to undergo a complete recovery from the electroporation procedure. We showed previously that regenerating muscle reproduces fetal AS patterns that return to the adult pattern by 16 days, when repair of severely damaged muscle is essentially complete (Orengo et al., 2011; Pedrotti et al., 2015). To evaluate the effect of MO delivery on the four selected endogenous AS events, we performed RT-PCR on mRNA samples from FDB muscles 7 or 14 days after vehicle injection and electroporation and from untouched FDBs and FDBs 23–26 days after injection/electroporation of control MO (control experimental condition in this manuscript). These experiments showed that, as expected, early after injection/electroporation with or without control MO, there is a switch to fetal AS patterns, but AS recovers to the adult pattern by 23–28 days (Figure S1A), when we performed our assays.

We evaluated the efficiency of redirected AS by RT-PCR on RNA isolated from FDB muscle. Densitometry quantification of PCR products revealed an almost complete switch to the short isoforms for the four events, without changes in non-targeted AS events, such as Bin1 and Vps39 (Figure 1C). All experiments included FDBs treated with a non-target control MO that we found did not affect muscle physiology or AS of the four events (Tmed2, Trip10, Snap23, and Tmed2) or Bin1 and Vps39 (Figure 1C). Further evidence of the specificity of redirected AS came from experiments in which we show that redirected AS

of only two events did not affect AS of the two non-targeted events (Figure S1B). Quantification of mRNA levels for Trip10, Snap23, Cltc, and Tmed2 (both bands) normalized to total Bin1 mRNA showed no significant differences, confirming that AS redirection occurred without changes in total mRNA levels (Figure S1C).

We confirmed efficient AS redirection at the protein level for Snap23 (33-nt exon) and Trip10 (168-nt exon; Figure 1D). Quantification of Trip10 and Snap23 total protein levels by densitometry revealed no significant changes, although a slight increase in Trip10 was evident after AS redirection (Figure S1D). This observation could be due to differences in protein stability or translation efficiencies because mRNA levels are unaltered. Two of our selected events (Cltc and Tmed2) involve small (21-nt) exons, making it difficult to separate the protein isoforms by western blot assays.

Taken together, these data demonstrated that our strategy allowed us to redirect multiple endogenous AS events in vivo simultaneously and with high efficiency.

Exclusive Expression of Short AS Variants Reduced Muscle Force Generation and Calcium Release

To understand the role of the protein isoform transitions of these trafficking genes in muscle physiology, we measured force generation and calcium release in whole-muscle bundles. We observed that, when short isoforms were exclusively expressed, calcium release and force generation were significantly reduced at all stimulation frequencies (Figures 2A and 2B). No changes in induced fatigue were detected (not shown). Whereas Snap23/Trip10 combination of AS redirection showed a similar trend to all four AS events, the dual combinations (Snap23/Trip10 or Cltc/Tmed2) of AS redirection were not significantly different than the control MO (Figure S2).

These results led us to investigate potential causes of reduced muscle force and calcium release generated by redirected AS of the four genes at the cellular level. We took two main avenues for our further studies, examination of T-tubule organization and mitochondria positioning, rationalizing that, during skeletal muscle postnatal development, both processes follow a similar time course and pattern (Boncompagni et al., 2009) and are key regulators of the ECC machinery.

Ultrastructure Characterization of FDB Muscles after Trafficking AS Redirection

Mitochondria are the main ATP sources during muscle contraction. Proper localization of mitochondria close to the SR is important for calcium handling and ECC. An anchoring system matures during skeletal muscle postnatal development that links mitochondria to the SR by tethers, forming a micro-domain for local bi-directional calcium signaling (Boncompagni et al., 2009). Therefore, we asked whether the abnormalities in calcium release and muscle force generation were due to changes in mitochondria content or localization within the myofibers.

Longitudinal sections of FDB muscles were evaluated by electron microscopy. We observed that sarcomere length was unchanged (1.9 μm; Figure S3A). In healthy skeletal muscle, mitochondria are mainly localized in pairs on either side of the Z lines throughout the

myofibrils and in small clusters at fiber periphery. In control animals, mitochondria were regularly aligned in pairs along Z lines, whereas the percentage of unpaired mitochondria lying at Z lines was significantly increased in animals injected with the MO mix (Figure S3B). A small but significant change was observed in the total number of mitochondria aligned along Z lines ($p = 0.05$), consistent with the increase percentage of unpaired mitochondria. We did not detect changes in the protein levels of the mitochondrial marker Cox subunit IV (Figure 1D), suggesting that mitochondria organization is altered without major changes in total mitochondria content. Electron microscopy images also revealed the more frequent presence of vesicle-like organelles in muscles where short Tmed2, Trip10, Snap23, and Cltc AS isoforms were almost exclusively expressed (Figure S3C). Overall, these results show that modulation of the four trafficking AS events increased the presence of vesicle-like organelles and induced mislocalization of mitochondria along Z lines.

AS Redirection Induced the Presence of More Centralized Nuclei and Myofiber Enlargement

We next examined myofiber morphology in cross section by H&E staining. We quantified the percentage of myofibers containing centralized nuclei and observed a significant increase after AS redirection compared with controls (7.3% ± 0.6% versus 4.9% ± 0.4%; $p = 0.004$; Figure 2C). Myofiber size can be evaluated by measuring the cross section area (CSA); however, these measurements can be distorted by the orientation of the sectioning angle. This is an important point in FDBs because they are small and difficult to manipulate during sectioning. This problem can be solved by measuring the minimum Feret's diameter, the minimum distance between two parallel tangents located at opposing borders of the myofiber (Briguet et al., 2004; Pertl et al., 2013). To avoid artifacts, we only measured fibers of 300–2,000 μm^2 and circularity between 0.70 and 1.00. We found that, in control samples, CSA and the minimum Feret's diameter exhibited a myofiber distribution with the same trend (Figure 2D, black). After AS modulation, we observed a significant increase in the proportion of fibers with the largest CSA and largest minimum Feret's diameter (≥28 μm) and a concomitant and significant decrease in the proportion of fibers with small CSA and minimum Feret's diameter (Figure 3D). Median CSA was also increased after AS modulation (503 ± 16 μm^2) compared with controls (420 ± 9 μm^2; $p = 0.0004$; Figure 2D, top). Similarly, median minimum Feret's diameter is higher after AS redirection (21.0 ± 0.2 μm) in comparison with controls (22.9 ± 0.4 μm; $p = 0.0012$; Figure 2D, bottom). We complement these results when we analyzed individual isolated fibers in terms of their area, length, diameter, and volume. AS redirection induced an increase in the proportion of bigger (area and volume), longer, and thicker myofibers and a decrease in the smaller, shorter, and thinner ones compared with controls (Figure 2E). In conclusion, AS redirection of the four selected events generated an increase in the percentage of fibers with centralized nuclei and significant changes in myofiber size distributions. Based on our findings, we hypothesized that AS redirection alters T-tubule organization and ECC, leading to the reduction in calcium release and muscle force generation.

T-tubule Organization Is Disrupted in FDB Myofibers after AS Modulation

Muscle contraction is the result of a finely and spatially regulated interplay between different ion channels within muscle fibers. In resting muscles, the Ryr1 at the SR is closed

because of the inhibitory action of the voltage-dependent calcium channel DHPR located in the T-tubules. DHPR opens in response to depolarization, propagating the action potential through the T-tubules deep into the muscle fibers. These signals induce Ryr1 opening and release of calcium from the SR, stimulating contraction. The reduction in calcium release and force generation (Figures 2A and 2B), together with the presence of enlarged myofibers, led us to investigate T-tubule organization and the localization of the Ryr1 and DHPR after AS redirection.

Isolated FDB myofibers were stained with FM4-64fx, and confocal microscopy revealed T-tubule disruption after AS redirection. Whereas FDB fibers from mice injected with control MO mainly exhibited a perfect regular T-tubule network, AS-redirected animals contained significantly more myofibers with disorganized T-tubules (Figure 3A). Two measurements were used to quantify the qualitative observations: (1) the normalized T-tubule power (Reynolds et al., 2013) and (2) the number of T-tubules per unit length (100 μm). Normalized T-tubule power was calculated after obtaining the fast Fourier transform (FFT) (Figure 3B). The first harmonic is the largest signal, and its power is an estimation of the spatial regularity, whereas its position is a measurement of the distance between T-tubules. The position of the first harmonic was similar for the myofibers from controls and those with AS redirection (control: 1.83 ± 0.01 μm; mix MO: 1.82 ± 0.01 μm). This result is in agreement with the constant sarcomere length measured by electron microscopy (Figure S3A). In contrast, the second and third harmonics observable in the control group were more frequently lost after AS redirection (Figure 3B), highlighting T-tubule disorganization. The ratio between the power of the first harmonic and its baseline is defined as the normalized T-tubule power (Reynolds et al., 2013; Figure 3B). AS redirection generated a shift in the distribution of fibers, with more fibers exhibiting lower T-tubule power (less regularity) in comparison with controls (Figure 3C). Consistently, the number of T-tubules per unit length (100 μm) was affected after AS redirection. Whereas, in control animals, 79% of the fibers contained ≥50 T-tubules per unit length and none of them had <44 T-tubules, in redirected AS mice, only 34% of the fibers had ≥50 T-tubules/100 μm ($p = 0.02$) and 33% of them had <44 T-tubules/100 μm ($p = 0.03$; Figure 3D). In conclusion, when short AS isoforms of Cltc, Tmed2, Snap23, and Trip10 are almost exclusively expressed, there is a significant increase in the proportion of myofibers where T-tubule network regularity is disrupted. These findings led us to examine the localization of two key players in ECC, the Ryr1 and DHPR, hypothesizing that T-tubule disorganization would mislocalize these molecules and thus impact their molecular functions.

Ryr1 and DHPR Are Mislocalized after AS Redirection

We performed immunofluorescence assays to determine the localization and colocalization of Ryr1 and DHPR. In FDBs isolated from mice injected with control MO, we found that DHPR and Ryr1 exhibited a regular striated pattern (Figure 4A, rows 1 and 2) and high levels of colocalization measured by Manders coefficients (M) ($M = 0.89 \pm 0.01$; $n = 18$; Figures 4B, top, and 4C, black). Similar plot profiles throughout a longitudinal line in the myofibers were obtained for Ryr1 and DHPR signals, reflecting their similar distribution and colocalization (Figure S4, top). Quantitatively, the majority of the myofibers (77% ± 6%) had $M \geq 0.88$ and none of them had $M < 0.80$ (Figure 4C, black). Results were

significantly different in the myofibers isolated from mice injected with the mix of MOs. We observed more fiber variability and a significant increase of those showing a loss of the Ryr1-DHPR regular pattern (Figure 4A, rows 3 and 4). Consistently, colocalization coefficients between Ryr1 and DHPR were significantly reduced ($M = 0.75 \pm 0.02$; $p = 2E–07$ versus control; $n = 30$; Figure 4C, red). In contrast to what we found in control mice, the majority of the redirected AS myofibers (55% ± 11%; $p = 0.04$ versus control) showed $M < 0.80$ and only a few of them (17% ± 8%; $p = 0.01$ versus control) showed $M \geq 0.88$ (Figure 4C, red). We next analyzed the number of DHPR peaks per unit length (100 μm) as we did for T-tubules. Results were in perfect agreement with those obtained for the T-tubules. DHPR staining showed doublet lines delimiting the two edges of each T-tubule. We did not have that definition for our T-tubule staining using FM-4-64fx. Therefore, whereas on average control, myofibers had 104 ± 1 DHPR peaks and 51 ± 1 T-tubules per unit length ($n = 18–23$), myofibers with AS redirection had significantly less DHPR peaks (93 ± 2; $p = 3E–05$ versus control; $n = 29$) and T-tubules (46 ± 1; $p = 0.002$ versus control; $n = 22$) per unit length (Figures S4C and 3D). The distribution analysis for the DHPR peaks per unit length was again consistent with all our data. Whereas the majority of the control myofibers (94% ± 6%) had ≥99 DHPR peaks per unit length and none of them had <90 DHPR peaks, AS-redirected fibers exhibited a shift of the distribution graph (30% ± 2% of them had <90 DHPR peaks and only 44% ± 7% had ≥99 DHPR peaks; $p \leq 0.01$ versus control).

To determine whether Ryr1 and DHPR protein levels were affected, we performed a quantitative assessment of their immunofluorescence signals in individual cells (Figure S5A) and immunofluorescence signal normalized to myofiber area (Figure S5B). We observed a significant higher Ryr1 and DHPR intensity after AS redirection that can be due to differences in myofiber size. However, whereas DHPR intensity normalized to fiber area showed no significant differences, Ryr1 intensity normalized to fiber area was still significantly higher after AS redirection (mix versus ctrl). This result might be due to a compensatory response to Ryr1 mislocalization and misfunction or to alterations in Ryr1 turnover. Taken together, these results demonstrate that AS redirection of four trafficking events disrupts T-tubule organization, leads to mislocalization of DHPR and Ryr1, and decreases calcium release and muscle force generation.

DISCUSSION

In this work, we linked three areas of research: trafficking, AS, and striated muscle physiology. Genome-wide studies have consistently shown the importance of transcriptional and post-transcriptional regulatory mechanisms in organ and tissue development and cell differentiation (Wang et al., 2008; Bland et al., 2010; Ellis et al., 2012; Merkin et al., 2012; Dillman et al., 2013; Giudice et al., 2014; Singh et al., 2014). The role of trafficking and membrane dynamics in striated muscle normal physiology and diseases is also well documented. However, the function of a vast number of trafficking proteins in muscle has not been explored. This is important because currently there are numerous muscle disorders with unknown causes. Although the physiological significance of AS regulation of trafficking and membrane-dynamics-related processes is an underexplored area, previous work definitely hints at its importance. For example, recently, AS misregulation of the sodium channel SCN5A has been shown to contribute to cardiac conduction delay and

arrhythmia in mice, similarly to what is observed in myotonic dystrophy (Freyermuth et al., 2016). Previously, mis-AS of Bin1 in mice has been associated with T-tubule alterations and skeletal muscle weakness, predominant features of myotonic dystrophy (Fugier et al., 2011).

Here, we investigated the physiological impact of AS of four trafficking genes in vivo: Snap23, Trip10, Cltc, and Tmed2. These four events have not been previously studied within physiological contexts. No human mutations were reported in these genes except two recently identified mutations in *CLTC* gene that lead to severe developmental defects (DeMari et al., 2016).

Using morpholinos, we redirected AS such that mostly the short isoforms (prevalent in neonates) were expressed in adult muscle. When only the short isoforms were expressed, calcium release was reduced as well as the muscle force generation (Figures 2A and 2B). A main regulator of skeletal muscle contractile functions is the precisely organized T-tubule and SR network. After AS redirection, muscle fibers were enlarged (Figures 2D and 2E) and T-tubule organization was significantly disrupted (Figure 3). In consequence, Ryr1 and DHPR lost their contact and coupling (Figure 4), suggesting that these four AS events impact ECC through T-tubule maintenance. Calcium release (reduced after AS redirection) is due to Ryr1 opening in response to the DHPR voltage sensing. In normal conditions, Ryr1 located at the SR is in close contact with the DHPR located at the T-tubules. When membrane is depolarized, DHPR sensor transmits this signal to Ryr1 and the channel is open, releasing calcium to the cytoplasm. When we modulated AS of our four events of interest, T-tubules are disorganized and thus DHPR and Ryr1 are also mislocalized, impairing the critical ECC, which could lead to the observed reduction in force generation and calcium release (Figure 5).

We propose that adult striated muscles require the long isoforms of Trip10 (membrane invagination and deformation), Snap23 (glucose metabolism and secretion), Tmed2 (cargo selection in secretion), and Cltc (endocytosis and actin scaffolding). Although we do not know the exact function of each of these isoforms, we demonstrated that these four AS isoforms are required for normal T-tubule maintenance, mitochondria localization, and ECC. When the long isoforms are not expressed, and instead the shortest ones are almost exclusively present, muscles are less efficient in terms of muscle force generation and calcium handling in comparison with control muscles.

It is possible that membrane deformations and invaginations important for T-tubules are affected by AS of Trip10. AS of Cltc and/or Snap23 can regulate intra-cellular transport of ion channels and receptors. Tmed2 and/or Snap23 AS may regulate secretion of growth factors important in muscle function and signaling. The functional role for each AS event in normal muscle function and structure still needs to be determined. Because these AS events are coordinately regulated during normal heart development (Giudice et al., 2014) and skeletal muscle myoblast cell differentiation (Singh et al., 2014), it is likely that all four trafficking events are required for proper skeletal muscle maintenance. We know that, in heart, these transitions occur during the first 4 postnatal weeks, when T-tubules are acquiring the full maturity (Giudice et al., 2014). T-tubule maturation and mitochondria positioning follow a similar time course and pattern during the first 3 or 4 postnatal weeks in skeletal

muscle development (Boncompagni et al., 2009). AS of trafficking genes seems to be temporally similar in striated muscle development. This information, together with our data, suggests that AS of trafficking and membrane dynamics genes are involved in T-tubule maturation and possibly in mitochondria positioning during the postnatal period of striated muscle development.

EXPERIMENTAL PROCEDURES

Detailed methods are available in the Supplemental Information.

Animals

Adult FvB wild-type male mice were used for the experiments. NIH guidelines for use and care of laboratory animals approved by Baylor College of Medicine (BCM) Institutional Animal Care and Use Committee were followed. Table S1 details the animals used.

MO Delivery

MOs (Gene Tools) sequences are detailed in Table S2. Hyaluronidase solution (0.5 mg/ml) was subcutaneously injected into FDB muscles (proximal-distal direction). After hyaluronidase injection (2–3 hr), mice were re-anesthetized and 300 μg total MO (control or mix) or 120 μg total MO (dual combinations) was injected. After 5 min, electrodes were placed subcutaneously at the proximal and distal FDB tendons to deliver 20 pulses of 150 V/cm, 20 ms in duration at 1 Hz frequency.

In Vitro Calcium and Force Measurements

FDB lateral and medial muscle bundles were dissected away, leaving the central muscle bundle and tendon. One end was attached to a fixed hook and the other to a force transducer. The muscle was placed in physiological saline solution continuously gassed with 95% O_2/5% CO_2 at 25°C and loaded with 5 μM Fura 4-F AM (Invitrogen). After 30 min, samples were rinsed with fresh solution and allowed to deesterify for 30 min. The optimal muscle length (L_o) and voltage (V_{max}) were adjusted to elicit maximum twitch force. Force-frequency characteristics were measured at stimulation frequencies of 1, 10, 20, 40, 80, 100, and 150 Hz every minute with pulse and train durations of 0.5 and 250 ms, respectively. Following a 5-min rest period, fatigue was assessed at 70 Hz (pulse 0.5 ms; train duration 400 ms; train rate 0.5 Hz). Fura 4-F AM excitation (360/380 nm) and emission (510 nm) were monitored simultaneously with force-frequency characteristics. After the contractile protocol, muscle length was measured and fiber bundles were trimmed of excess muscle and connective tissue, blotted dry, and weighed. Muscle weight and L_o were used to estimate CSA and to calculate absolute forces (Close, 1972) expressed as N/cm^2. The 360/380 nm ratio was calculated to determine intracellular calcium changes during FDB stimulation.

FDB Myofiber Isolation

FDB muscles were digested with 4 mg/ml Collagenase A in DMEM supplemented with 10% fetal bovine serum, 1% penicillin/streptomycin at 37°C under 5% CO_2. After 2–3 hr, myofibers were obtained by careful trituration using glass pipettes with decreasing

diameters. Isolated myofibers were placed in fresh medium and incubated at 37°C overnight. The next day, cells were utilized for the assays.

Western Blots

After myofiber isolation, protein was extracted using Ripa buffer and western blots were performed. Primary antibodies (rabbit polyclonal) dilutions were anti-Snap23 (1:500), anti-Cip4 (1:1,000), anti-sarcomeric alpha-actinin (1:500), and anti-Cox IV subunit (1:1,000).

RT-PCR Assays

RNA was isolated using Trizol, and RT reactions were performed using the High Capacity cDNA RT Kit (Applied Biosystems) following manufacturer protocols. PCRs were performed using GoTaq DNA Polymerase (Promega). Quantification was performed by densitometry using ImageJ plugin for gel analysis.

T-tubule Staining

Isolated myofibers were washed with Hank's Balanced Salt Solution and stained with 5 μg/ml FM4-64fx (Life Technologies) for 30 min. Samples were washed twice, fixed in 4% paraformaldehyde, and stained with 2 μM DAPI.

Confocal Microscopy

Confocal microscopy was performed using a Nikon A1-Rs inverted laser scanning microscope.

Image Processing and Quantitative Analysis

Image processing and quantitative analysis were performed using ImageJ (https://imagej.nih.gov) and/or Fiji (Fiji is Just ImageJ; Schindelin et al., 2012; http://imagej.net/Fiji/Downloads) softwares.

Statistics

Data are reported as mean ± SEM. p values were estimated by a Student's t test (two tailed) for all the experiments except the force and calcium measurements (one-way ANOVA) and the median CSA and minimum Feret's diameter analyses (Kruskal Wallis non-parametric test). $p \leq 0.05$ was considered significant.

Supplementary Material

Refer to Web version on PubMed Central for supplementary material.

Acknowledgments

We thank Ravi Singh and Marissa Ruddy Scavuzzo (BCM) for advice with initial immunofluorescence experiments and help with RT-PCRs in gastrocnemius, respectively. This project has been supported by NIH grants R01AR045653 (to T.A.C.), R01HL045565 (to T.A.C.), R01AR060733 (to T.A.C.), and R01AR061370 (to G.G.R.); American Heart Association Postdoctoral Fellowship 14POST20270001 (to J.G.); The University of North Carolina at Chapel Hill startup package (to J.G.); and NIH fellowship T32HL007676 (to J.A.L.). The Integrated Microscopy Core at BCM also supported this project with funding from NIH (HD007495, DK56338, and CA125123), the Dan L. Duncan Cancer Center (NIH P30CA125123), and the John S. Dunn Gulf Coast Consortium for Chemical

Genomics. This work was supported in part also by the Public Health Service grant DK56338, which funds the Texas Medical Center Digestive Diseases Center.

References

Bland CS, Wang ET, Vu A, David MP, Castle JC, Johnson JM, Burge CB, Cooper TA. Global regulation of alternative splicing during myogenic differentiation. Nucleic Acids Res. 2010; 38:7651–7664. [PubMed: 20634200]

Blencowe BJ. Alternative splicing: new insights from global analyses. Cell. 2006; 126:37–47. [PubMed: 16839875]

Boncompagni S, Rossi AE, Micaroni M, Beznoussenko GV, Polishchuk RS, Dirksen RT, Protasi F. Mitochondria are linked to calcium stores in striated muscle by developmentally regulated tethering structures. Mol Biol Cell. 2009; 20:1058–1067. [PubMed: 19037102]

Boström P, Andersson L, Rutberg M, Perman J, Lidberg U, Johansson BR, Fernandez-Rodriguez J, Ericson J, Nilsson T, Borén J, Olofsson SO. SNARE proteins mediate fusion between cytosolic lipid droplets and are implicated in insulin sensitivity. Nat Cell Biol. 2007; 9:1286–1293. [PubMed: 17922004]

Boström P, Andersson L, Vind B, Håversen L, Rutberg M, Wickström Y, Larsson E, Jansson PA, Svensson MK, Brånemark R, et al. The SNARE protein SNAP23 and the SNARE-interacting protein Munc18c in human skeletal muscle are implicated in insulin resistance/type 2 diabetes. Diabetes. 2010; 59:1870–1878. [PubMed: 20460426]

Briguet A, Courdier-Fruh I, Foster M, Meier T, Magyar JP. Histological parameters for the quantitative assessment of muscular dystrophy in the mdx-mouse. Neuromuscul Disord. 2004; 14:675–682. [PubMed: 15351425]

Buljan M, Chalancon G, Eustermann S, Wagner GP, Fuxreiter M, Bateman A, Babu MM. Tissue-specific splicing of disordered segments that embed binding motifs rewires protein interaction networks. Mol Cell. 2012; 46:871–883. [PubMed: 22749400]

Close RI. Dynamic properties of mammalian skeletal muscles. Physiol Rev. 1972; 52:129–197. [PubMed: 4256989]

DeMari J, Mroske C, Tang S, Nimeh J, Miller R, Lebel RR. CLTC as a clinically novel gene associated with multiple malformations and developmental delay. Am J Med Genet A. 2016; 170A:958–966. [PubMed: 26822784]

Dillman AA, Hauser DN, Gibbs JR, Nalls MA, McCoy MK, Rudenko IN, Galter D, Cookson MR. mRNA expression, splicing and editing in the embryonic and adult mouse cerebral cortex. Nat Neurosci. 2013; 16:499–506. [PubMed: 23416452]

Dowling JJ, Gibbs EM, Feldman EL. Membrane traffic and muscle: lessons from human disease. Traffic. 2008; 9:1035–1043. [PubMed: 18266915]

Ellis JD, Barrios-Rodiles M, Colak R, Irimia M, Kim T, Calarco JA, Wang X, Pan Q, O'Hanlon D, Kim PM, et al. Tissue-specific alternative splicing remodels protein-protein interaction networks. Mol Cell. 2012; 46:884–892. [PubMed: 22749401]

Foster LJ, Yaworsky K, Trimble WS, Klip A. SNAP23 promotes insulin-dependent glucose uptake in 3T3-L1 adipocytes: possible interaction with cytoskeleton. Am J Physiol. 1999; 276:C1108–C1114. [PubMed: 10329959]

Freyermuth F, Rau F, Kokunai Y, Linke T, Sellier C, Nakamori M, Kino Y, Arandel L, Jollet A, Thibault C, et al. Splicing misregulation of SCN5A contributes to cardiac-conduction delay and heart arrhythmia in myotonic dystrophy. Nat Commun. 2016; 7:11067. [PubMed: 27063795]

Fugier C, Klein AF, Hammer C, Vassilopoulos S, Ivarsson Y, Toussaint A, Tosch V, Vignaud A, Ferry A, Messaddeq N, et al. Misregulated alternative splicing of BIN1 is associated with T tubule alterations and muscle weakness in myotonic dystrophy. Nat Med. 2011; 17:720–725. [PubMed: 21623381]

Giudice J, Xia Z, Wang ET, Scavuzzo MA, Ward AJ, Kalsotra A, Wang W, Wehrens XHT, Burge CB, Li W, et al. Alternative splicing regulates vesicular trafficking genes in cardiomyocytes during post-natal heart development. Nat Commun. 2014; 5:3603. [PubMed: 24752171]

Jerome-Majewska LA, Achkar T, Luo L, Lupu F, Lacy E. The trafficking protein Tmed2/p24beta(1) is required for morphogenesis of the mouse embryo and placenta. Dev Biol. 2010; 341:154–166. [PubMed: 20178780]

Kawanishi M, Tamori Y, Okazawa H, Araki S, Shinoda H, Kasuga M. Role of SNAP23 in insulin-induced translocation of GLUT4 in 3T3-L1 adipocytes. Mediation of complex formation between syntaxin4 and VAMP2. J Biol Chem. 2000; 275:8240–8247. [PubMed: 10713150]

Merkin J, Russell C, Chen P, Burge CB. Evolutionary dynamics of gene and isoform regulation in Mammalian tissues. Science. 2012; 338:1593–1599. [PubMed: 23258891]

Orengo JP, Ward AJ, Cooper TA. Alternative splicing dysregulation secondary to skeletal muscle regeneration. Ann Neurol. 2011; 69:681–690. [PubMed: 21400563]

Pan Q, Shai O, Lee LJ, Frey BJ, Blencowe BJ. Deep surveying of alternative splicing complexity in the human transcriptome by high-throughput sequencing. Nat Genet. 2008; 40:1413–1415. [PubMed: 18978789]

Pedrotti S, Giudice J, Dagnino-Acosta A, Knoblauch M, Singh RK, Hanna A, Mo Q, Hicks J, Hamilton S, Cooper TA. The RNA-binding protein Rbfox1 regulates splicing required for skeletal muscle structure and function. Hum Mol Genet. 2015; 24:2360–2374. [PubMed: 25575511]

Pertl C, Eblenkamp M, Pertl A, Pfeifer S, Wintermantel E, Lochmüller H, Walter MC, Krause S, Thirion C. A new web-based method for automated analysis of muscle histology. BMC Musculoskelet Disord. 2013; 14:26. [PubMed: 23324401]

Reynolds JO, Chiang DY, Wang W, Beavers DL, Dixit SS, Skapura DG, Landstrom AP, Song LS, Ackerman MJ, Wehrens XHT. Junctophilin-2 is necessary for T-tubule maturation during mouse heart development. Cardiovasc Res. 2013; 100:44–53. [PubMed: 23715556]

Rusconi F, Thakur H, Li J, Kapiloff MS. CIP4 is required for the hypertrophic growth of neonatal cardiac myocytes. J Biomed Sci. 2013; 20:56. [PubMed: 23915320]

Schindelin J, Arganda-Carreras I, Frise E, Kaynig V, Longair M, Pietzsch T, Preibisch S, Rueden C, Saalfeld S, Schmid B, et al. Fiji: an open-source platform for biological-image analysis. Nat Methods. 2012; 9:676–682. [PubMed: 22743772]

Sigismund S, Confalonieri S, Ciliberto A, Polo S, Scita G, Di Fiore PP. Endocytosis and signaling: cell logistics shape the eukaryotic cell plan. Physiol Rev. 2012; 92:273–366. [PubMed: 22298658]

Singh RK, Xia Z, Bland CS, Kalsotra A, Scavuzzo MA, Curk T, Ule J, Li W, Cooper TA. Rbfox2-coordinated alternative splicing of Mef2d and Rock2 controls myoblast fusion during myogenesis. Mol Cell. 2014; 55:592–603. [PubMed: 25087874]

Vassilopoulos S, Gentil C, Lainé J, Buclez PO, Franck A, Ferry A, Précigout G, Roth R, Heuser JE, Brodsky FM, et al. Actin scaffolding by clathrin heavy chain is required for skeletal muscle sarcomere organization. J Cell Biol. 2014; 205:377–393. [PubMed: 24798732]

Wang ET, Sandberg R, Luo S, Khrebtukova I, Zhang L, Mayr C, Kingsmore SF, Schroth GP, Burge CB. Alternative isoform regulation in human tissue transcriptomes. Nature. 2008; 456:470–476. [PubMed: 18978772]

Yan S, Lv Z, Winterhoff M, Wenzl C, Zobel T, Faix J, Bogdan S, Grosshans J. The F-BAR protein Cip4/Toca-1 antagonizes the formin Diaphanous in membrane stabilization and compartmentalization. J Cell Sci. 2013; 126:1796–1805. [PubMed: 23424199]

Highlights

- Adult trafficking genes isoforms are expressed in adult skeletal muscle
- Splicing of four trafficking genes is redirected to their fetal isoforms in vivo
- Fetal isoforms of trafficking genes impair calcium handling and muscle force
- Adult isoforms of trafficking genes are required for excitation-contraction coupling

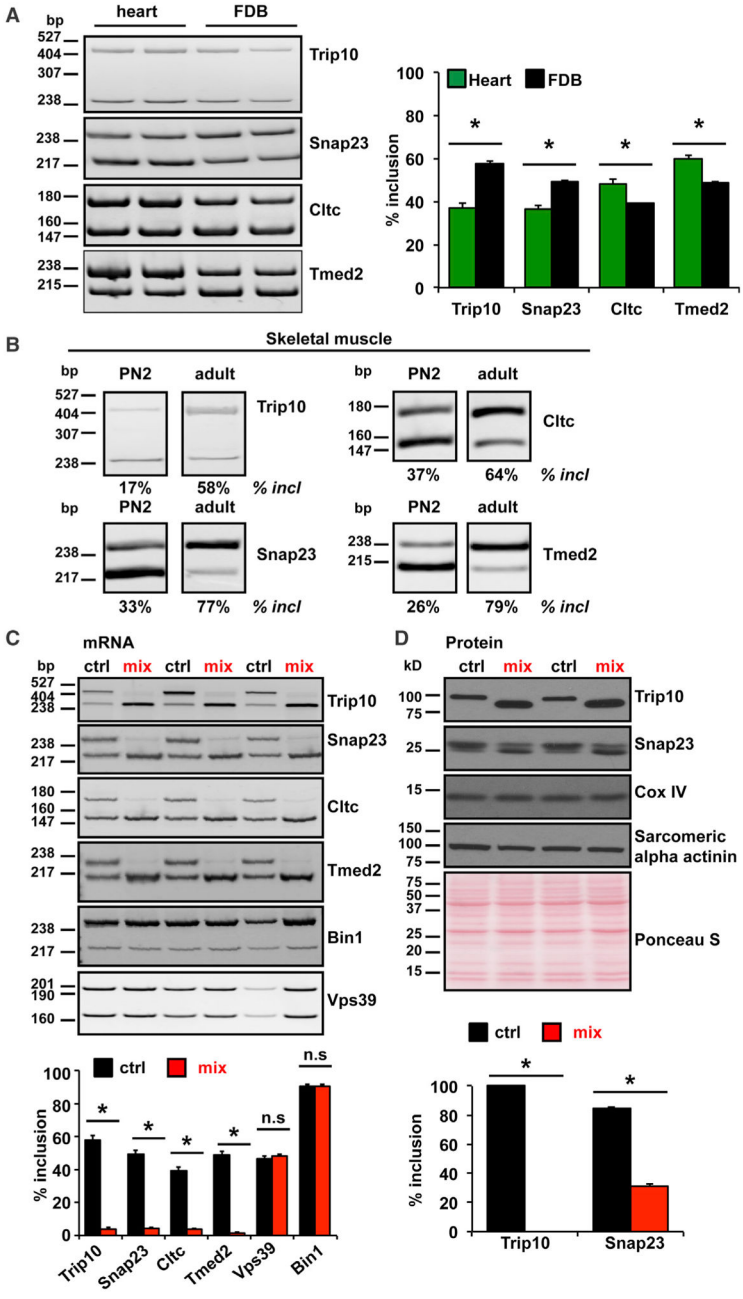

Figure 1. Modulation of Endogenous AS In Vivo Is Highly Efficient

(A) Quantitation of the percent of inclusion (% incl) by RT-PCR. *p ≤ 0.05 (t test); n = 20–22 (FDB); n = 3 (heart). Results are mean ± SEM.

(B) RT-PCR assays on skeletal muscles at postnatal day 2 (PN2) (forelimbs: Trip10; gastrocnemius: rest) and adult stages (triceps: Trip10; gastrocnemius: rest). Panels for each event come from the same gel.

(C and D) FDBs were isolated 3 weeks after MO delivery and analyzed by RT-PCR (C) or western blot (D) assays. *p ≤ 0.05 (t test); n = 20–22 (RT-PCRs: Snap23; Trip10; Cltc;

Tmed2; and Vps39); n = 8–9 (RT-PCRs: Bin1); n = 3 (western blots). Results are mean ± SEM. n.s., not significant.

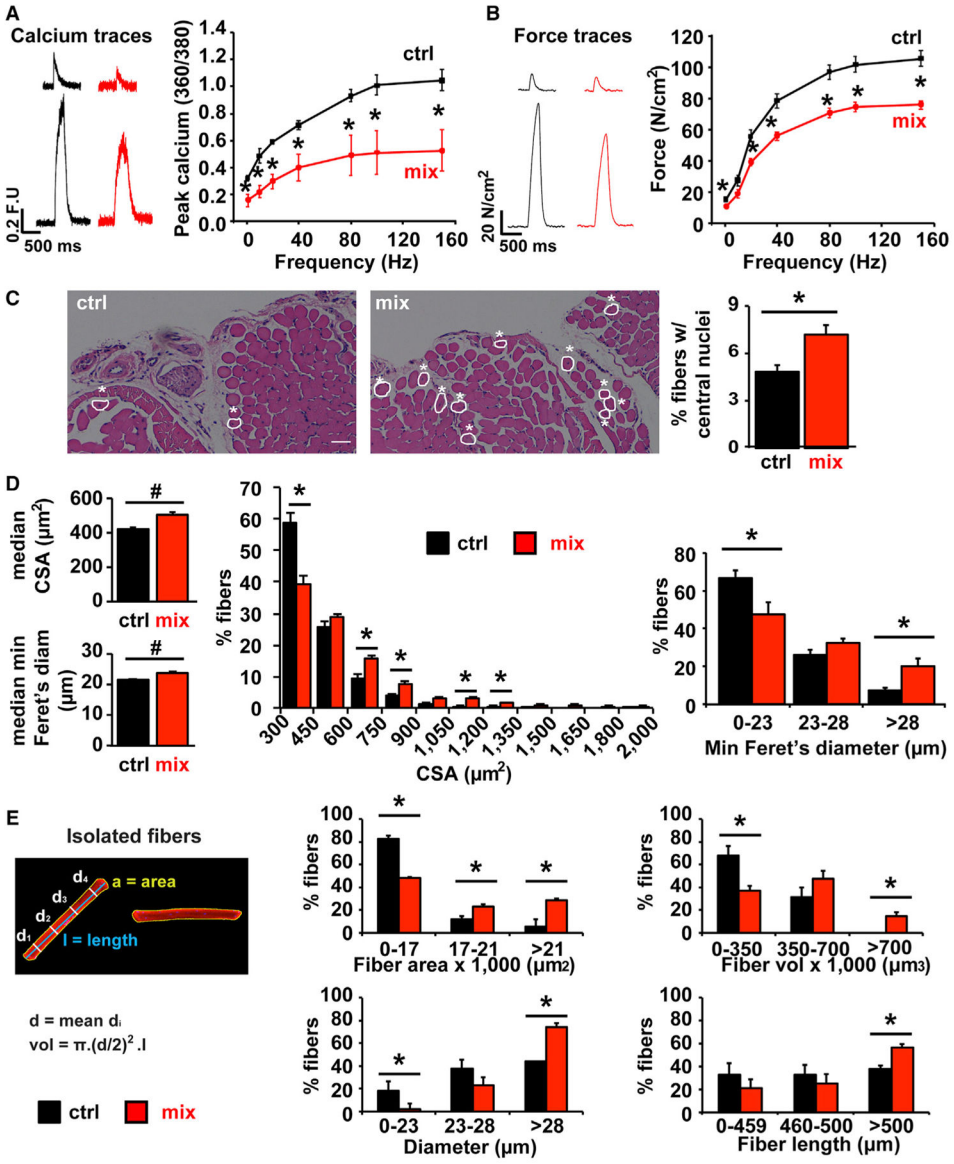

Figure 2. AS Modulation Reduces Muscle Force Generation and Calcium Release and Induces Centralized Nuclei and Myofiber Enlargement

(A) Representative calcium tracing following 1-Hz and 150-Hz stimulations (control, black; mix MO, red). Fura 4-F excitation ratio (360/380 nm) and emission (510 nm) were monitored simultaneously with force-frequency characteristics analysis.

(B) Representative force tracing following 1-Hz and 150-Hz stimulations (control, black; mix MO, red). Force-frequency characteristics were measured at stimulation frequencies of 1, 10, 20, 40, 80, 100, and 150 Hz every minute. Force was normalized to the CSA. *p ≤ 0.05 (ANOVA); n = 3–4 animals/condition.

(C) FDB samples were analyzed by H&E staining and bright field microscopy (10× objective). Percentage of myofibers with centralized nuclei was measured. *p ≤ 0.05; n = 46 (controls) or 28 images (mix MO); three animals/condition. The scale bars represent 50 µm.

(D) CSA and minimum Feret's diameter (min Feret diam). *p ≤ 0.05 (t test); #p ≤ 0.05 (Kruskal Wallis non-parametric test); n = 30–210 fibers/image; 10–14 images/condition; six animals/condition.

(E) FDB myofibers were immunostained and imaged by confocal microscopy (10× objective). *p ≤ 0.05 (t test); n = 57–67 fibers/condition; three animals/condition. Results are mean ± SEM or median ± SEM. vol, volume.

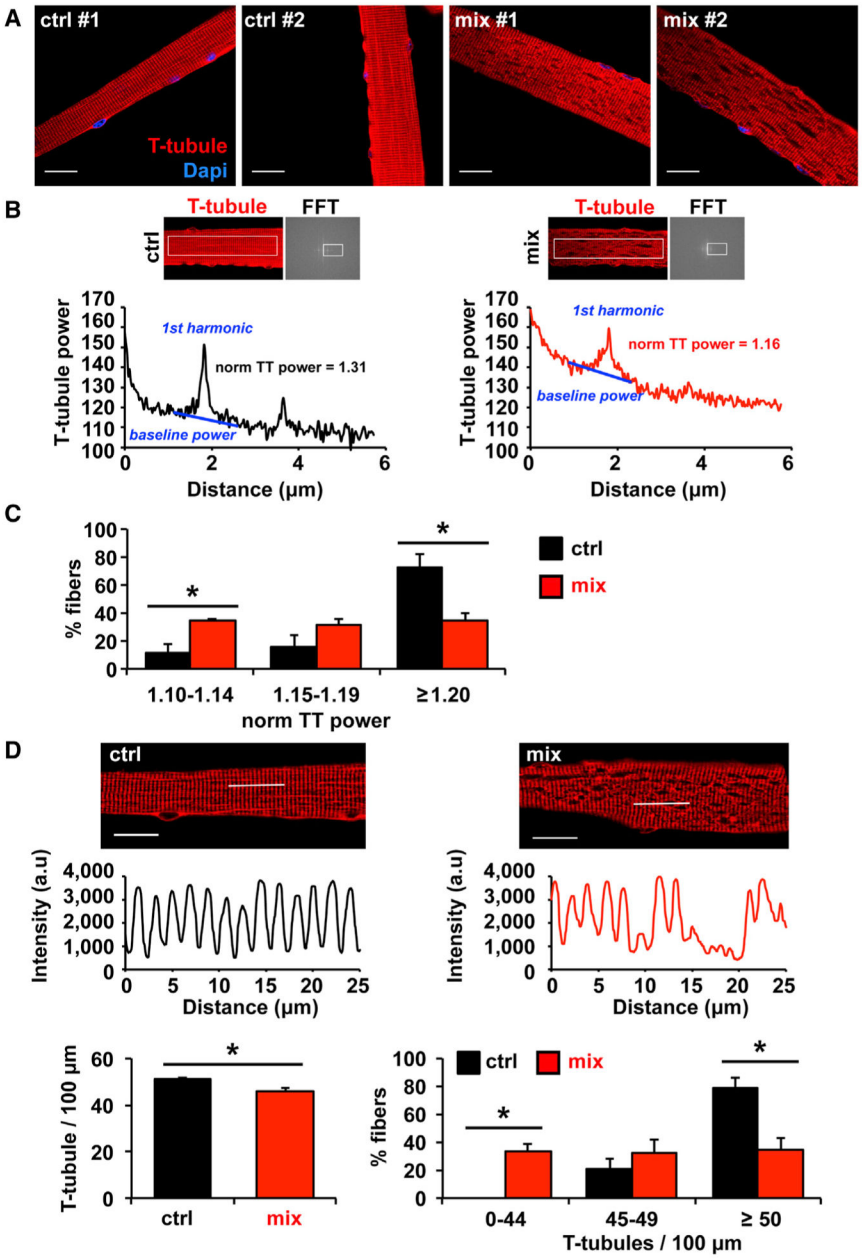

Figure 3. T-tubule Organization Is Disrupted in FDB Myofibers after AS Modulation

(A) FDB myofibers were enzymatically isolated, stained with 5 μg/ml FM4-64 fx, fixed, and imaged by confocal microscopy (100× objective).

(B and C) Normalized T-tubule power (norm TT power) was defined as the ratio between the first harmonic power and the baseline (B). Distribution histograms are shown (C).

(D) Confocal images were used to compute plots along longitudinal lines within the myofibers. We measured the number of picks (T-tubules) per unit length (100 μm). *p ≤0.05 (t test); n = 22–23 fibers/condition; three animals/condition. Results are mean ± SEM. The scale bars represent 20 μm.

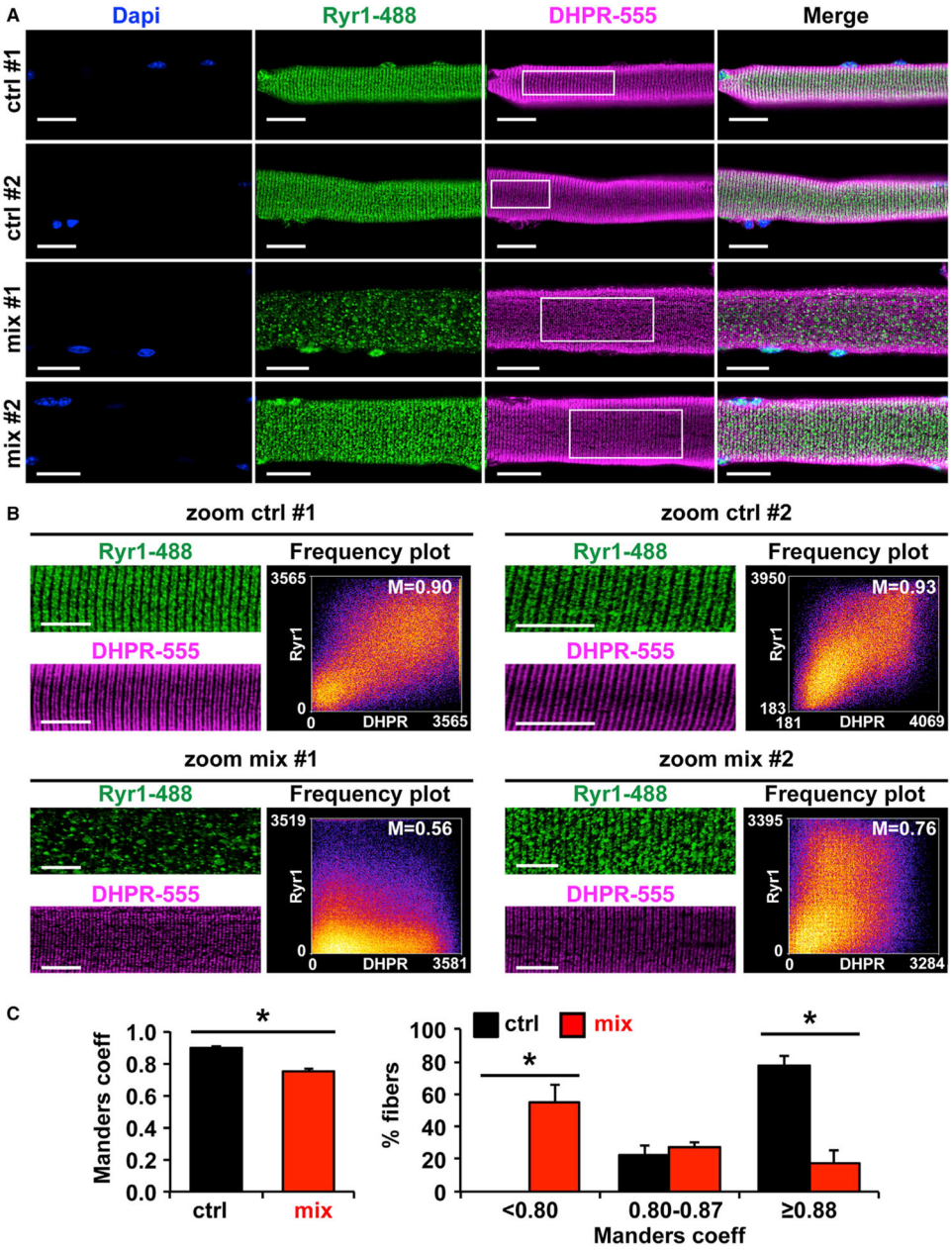

Figure 4. Ryr 1 and DHPR Are Mislocalized after AS Redirection

(A) FDB myofibers were immunostained (Ryr1, green; DHPR, magenta). The scale bars represent 20 μm.

(B) Colocalization Manders coefficients (M) and frequency plots were obtained on the region of interest (white rectangles in A). The scale bars represent 10 μm.

(C) Distribution of Manders coefficients within the myofiber population. *p ≤0.05 (t test); n = 18 (control) or 23 (mix MO) fibers; three animals/condition. Results are mean ± SEM.

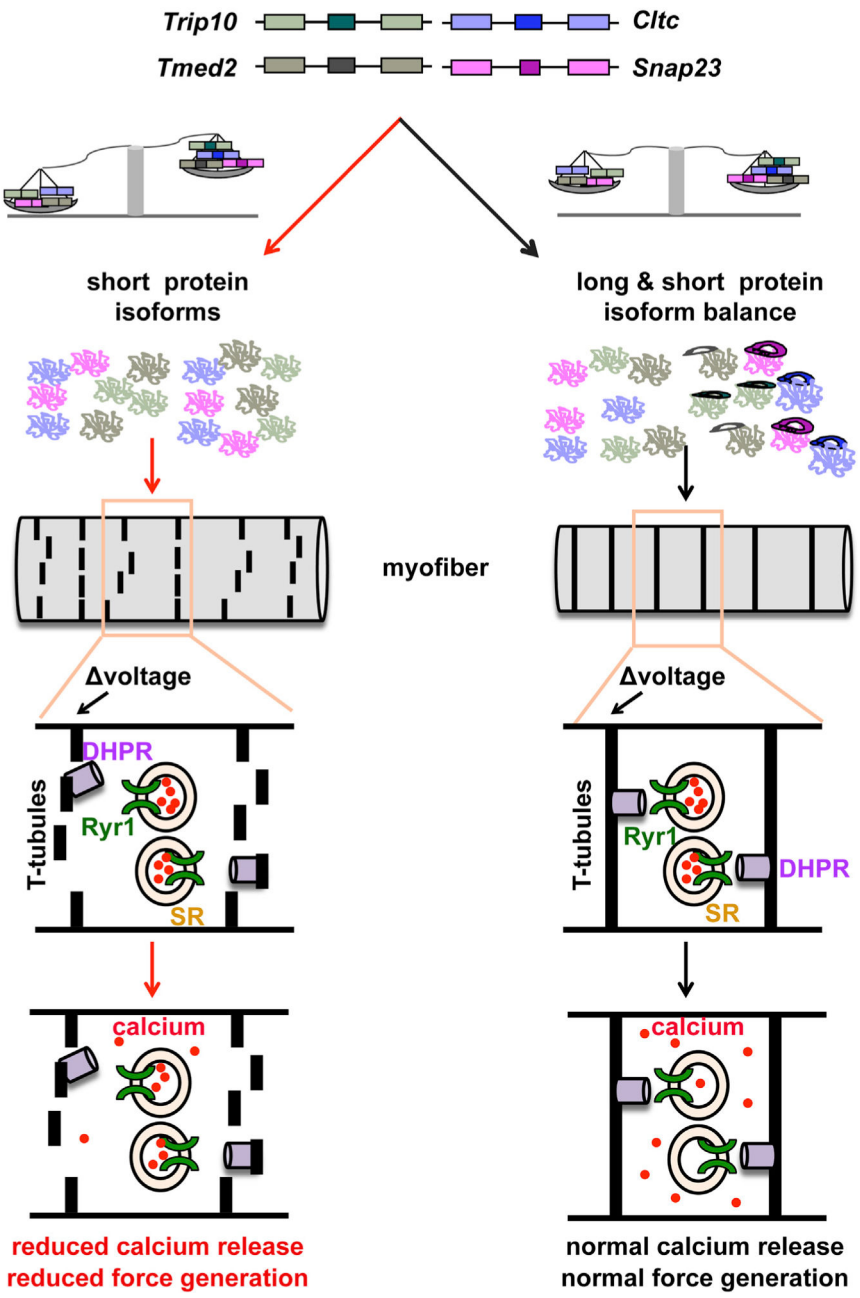

Figure 5. Summary

AS redirection of four trafficking events impacts on T-tubule organization, fiber size, Ryr1 and DHPR localization, and colocalization. In consequence, muscle force generation and calcium release are reduced.